

In press at Bound. Layer Meteorol, May 1999

**On momentum flux and velocity spectra over waves**

WILLIAM M. DRENNAN

*Rosenstiel School of Marine and Atmospheric Science, University of Miami, FL, USA*

KIMMO K. KAHMA

*Finnish Institute of Marine Research, Helsinki, Finland*

MARK A. DONELAN\*

*Rosenstiel School of Marine and Atmospheric Science, University of Miami, FL, USA*

Manuscript Submitted 21 July 1998, 26 January 1999

---

\* Also: Emeritus scientist, National Water Research Institute, Canada Centre for Inland Waters, Burlington, Ontario, Canada

---

*Corresponding author address:* Dr. W.M. Drennan, Department of Applied Marine Physics, Rosenstiel School of Marine and Atmospheric Science, University of Miami, 4600 Rickenbacker Causeway, Miami, FL 33149-1098, USA. Email: wdrennan@rsmas.miami.edu

**DISTRIBUTION STATEMENT A**  
**Approved for Public Release**  
**Distribution Unlimited**

DTIC QUALITY INSPECTED 4

19990709 057

## ABSTRACT

Data from a research tower in Lake Ontario are used to study the validity of Monin-Obukhov scaling in the marine atmospheric boundary layer under various wave conditions. It is found that over pure wind seas, the velocity spectra and cospectra follow established universal scaling laws. However in the presence of swells outrunning weak winds, velocity spectra and co-spectra no longer satisfy universal spectral shapes. Here, Monin-Obukhov similarity theory, and the classical logarithmic boundary layers are no longer valid. It is further shown that in the presence of such swells the momentum flux can be significantly modified over pure wind sea values. The implications of these findings for bulk flux estimations and on the inertial dissipation method for calculating fluxes are discussed.

Keywords: Air-sea fluxes, wind stress, wind waves, swell, universal spectra, Monin-Obukhov theory

## 1. Introduction

The basis of most recent work on turbulence in the atmospheric surface layer lies in the ideas first proposed by Obukhov (1946) and Monin and Obukhov (1954). In stationary and homogeneous conditions, the stress  $\tau$  is assumed to be constant in a region near the interface, but well above the viscous sublayer. Here, the stress is given by

$$\tau = -\rho \overline{u'w'} = \rho u_*^2, \quad (1)$$

where  $u'$  and  $w'$  are the horizontal (in line with the mean wind) and vertical components of the turbulent fluctuations of the wind field,  $\rho$  is the air density, and the overbar represents time averaging. In Monin-Obukhov (MO) similarity theory the friction velocity,  $u_*$ , is introduced as a velocity scale. In neutral conditions, with the assumption of eddy viscosity increasing linearly with height  $z$  and friction velocity, this leads to the well known logarithmic velocity profile of a shear layer.

More generally, buoyancy is an additional source (or sink) of turbulence. An important consequence of Monin-Obukhov (MO) similarity theory is that buoyancy can be brought into the above picture through the addition of a single length scale  $L$ , the Obukhov length:

$$L = \frac{-u_*^3}{\kappa g (\overline{w'\theta'}/T_o + 0.61 \overline{w'q'})}, \quad (2)$$

where  $\kappa$  is the dimensionless von Kármán constant,  $g$  is the gravitational constant,  $T_o$  the reference absolute temperature, and  $\theta'$  and  $q'$  are the turbulent fluctuations of potential temperature and specific humidity respectively. The Obukhov length represents the height at which mechanical (shear) and buoyant forcing are equal. It follows from MO theory that

$$\frac{\partial U}{\partial z} \frac{\kappa z}{u_*} = \phi_u(\zeta) \quad (3)$$

where  $\zeta = z/L$ . Integrating (3), the velocity profile is

$$\frac{(U_z - U_s)}{u_*} = \frac{1}{\kappa} \left[ \ln\left(\frac{z}{z_o}\right) - \psi_u(\zeta) \right]. \quad (4)$$

where  $U_z$  is the mean wind speed at  $z$  meters,  $U_s$  the mean surface velocity,  $z_o$  is the roughness length, where  $U_{z_o} = U_s$ , and

$$\psi_u = \int_{\zeta_o}^{\zeta} \frac{[1 - \phi_u(\zeta)]}{\zeta} d\zeta. \quad (5)$$

In neutral conditions,  $\zeta \rightarrow 0$ ,  $\phi_u \rightarrow 1$  and  $\psi_u \rightarrow 0$ , yielding the classical logarithmic profile shape.

Since the introduction of MO theory, considerable work has been carried out to determine the dimensionless function  $\phi_u$  and the von Kármán constant. Early experimental verification of MO similarity in the atmosphere over land was given by Zilitinkevich and Chalikov (1968), Dyer and Hicks (1970) and Businger *et al.* (1971). Högström (1996) provides a summary of more recent work. If, as suggested by Yaglom (1977), the various results are normalised so that  $\kappa = 0.4$ , Högström (1996) finds good agreement amongst many experiments.

Although very little profile data over water have been presented to date, it is generally assumed that the profile relations over the ocean are identical to those over land (c.f. Large and Pond 1981, Yelland and Taylor 1996). However, it has long been recognised that the physics at the air-sea interface are significantly different from those at an air-land interface (Stewart 1961). Over the sea, energy and momentum are transferred from the winds to the surface, resulting in waves and surface currents. As the waves evolve the surface roughness changes, hence the air flow over the ocean surface is coupled with the evolution of the surface itself. In particular, near the sea surface (again, away from the viscous sublayer) the stress is made up not only of a turbulent component, but also of a wave-induced component,  $\tau^w$ , where this latter component accounts for the transfer of momentum to the waves (Janssen 1989). Away from the surface the turbulent stress dominates, while the wave induced stress is increasingly important near the surface. Given that the total stress,  $\tau = \tau^w - \overline{\rho u'w'}$ , is constant, the increase in  $\tau^w$  near the surface is balanced by a reduction in the turbulent stress. Hence in this region the

velocity profiles (supported by the turbulent stress) are expected to deviate from their over-land shapes (4) (Stewart 1961).

Using an empirical wave model, Janssen (1989) estimated the thickness of the wave boundary layer (WBL, where the wave induced stress is significant) to be  $u_*^2/g \approx O(0.1\text{m})$  for young waves; less for mature waves. Makin and Mastenbroek (1996) estimate  $\tau^w$  to be under 5% of the total stress at the height of 1 m, under 1% by 3 m (for  $U = 15 \text{ ms}^{-1}$ ). These estimates, made assuming pure unimodal wind seas, indicate that the WBL lies below typical measurement heights in the field. Hence, we might expect that measured profiles over the sea would be similar to those over land. Indeed, recent open ocean results of Edson and Fairall (1998), based on data estimated to have been taken above the WBL, show strong support for MO similarity in the marine atmospheric surface layer. There are, however, indications that this is not always the case. Holland *et al.* (1981) presented unpublished data from the Donelan *et al.* (1974) experiment showing profiles where the wind speed *increased* from a height of 12.3 m down to 2.4 m. In the case presented, relatively light winds were blowing in the same direction as a strong swell. Similar results, under similar conditions, were reported recently by Smedman *et al.* (1999). Hence, departures from MO similarity have been observed over waves.

This has particular significance with respect to efforts to determine the so-called bulk relations by which one can estimate surface fluxes from more readily measured values, such as mean wind speeds and temperatures. This is important in improving the accuracy of atmospheric and oceanic models, which are often limited by sparseness of reliable boundary data. The drag coefficient, relating the momentum flux to the mean wind speed, is  $C_{Dz} = \tau/(\rho(U_z - U_s)^2)$ . According to MO theory,  $C_{Dz} = f(z/z_o, \zeta)$ , which follows from (4). It is standard practice to eliminate the dependence on stability and height by considering the neutral drag coefficient at a reference height of 10m,

$C_{D10N} = \tau / (\rho(U_{10N} - U_s)^2)$ , where  $U_{zN} = U_z + (u_*/\kappa)\psi_u(\zeta)$ . Hence,  $C_{D10N}$  is expected to be a function of the roughness alone.

Using dimensional arguments, Charnock (1955) proposed the relation  $z_o = \alpha u_*^2/g$ , where  $\alpha$ , the Charnock constant, is of order 0.01. The resultant dependence of  $C_{D10N}$  on wind speed was confirmed by Smith (1980). More recently it has been shown that  $C_{D10N}$  is also dependent on wave age (Donelan 1990; Smith *et al.* 1992; Donelan *et al.* 1993), implying that  $\alpha$  is in fact a function of wave age. This was first proposed by Kitaigorodskii and Volkov (1965).

However, it is evident that scatter in experimental determinations of  $C_{D10N}$  can not be explained by variability in wind speed and wave age alone. One factor which has been proposed to account for some of the observed scatter is swell. Geernaert *et al.* (1986), Donelan *et al.* (1997) and Rieder (1997) all report increased variability in the drag coefficient in the presence of background swells. Donelan *et al.* (1997) and Drennan *et al.* (1999) presented evidence showing that strong swells (those whose energy greatly exceeds that of the wind sea) running against light-moderate winds were associated with  $C_{D10N}$  values significantly enhanced over pure wind sea values. In contrast, Dobson *et al.* (1994) and Yelland and Taylor (1996) reported no effect of swell on the drag coefficient. Smith *et al.* (1996), in their review of air-sea fluxes, conclude that the coupling of the stress and swell remains an area for future research, especially in the open sea.

Here we investigate the hypothesis that the presence of swell can significantly alter the drag coefficient, and that these changes cannot be modelled within the framework of traditional MO theory. In particular in these conditions, in which the swell introduces into the problem an additional length scale, MO theory would appear to fail. The outline of the paper is as follows. In section 2 we describe an experiment in which eddy-correlation stress and other supporting data were collected at a tower in Lake Ontario. In section 3, the analysis methods are described. In the following sections,

results are presented for both pure wind sea and mixed seas (swell plus wind sea). Some implications of the results are discussed in section 6, and conclusions are presented in section 7.

## 2. The WAVES experiment

During the autumn seasons of 1985-1987, the WAVES (Water-Air Vertical Exchange Study) experiments were carried out from the National Water Research Institute (NWRI) research tower in Lake Ontario. The tower was designed specifically for air-sea interaction research, with minimal disturbance to both wind and waves (see Figure 1). It is located in 12 m of water, 1100 m from the western shore of the lake (Figure 2), and is connected to an onshore trailer via underground cable. Wave heights at the tower have been measured in excess of 6 m in strong easterly (long fetch) winds, whereas heights of less than 1 m are typical in strong westerly (short fetch) blows.

During the WAVES experiments, the tower was equipped to study the turbulence budgets on both sides of the interface. A full description of the air-side apparatus is provided in Donelan *et al.* (1999), while the water-side turbulence measurements are discussed in Terray *et al.* (1996).

We describe here the instruments relevant to this study. A Gill anemometer-bivane (R.M. Young) was mounted on a mast on the tower (Figure 1), and yielded the three components of the wind vector, and thence the wind stress vector, at a height of approximately 12 m. The bivane's anemometer was calibrated using the 100 m long towing carriage current meter calibration facility at NWRI. The signals from the bivane anemometer were corrected for frequency response of both the styrofoam propeller (Hicks 1972) and vane (MacCready and Jex 1964). Wind tunnel tests carried out at NWRI indicate a propeller distance constant of 1 m. The damping coefficient and natural wavelength of oscillation for the second order vane correction were found to be 0.52 and 5.8 m respectively. The separation distance between the propeller and vane is

0.73 m. Sensors for temperature and humidity were also located on the mast at about 12 m.

Near the surface, high frequency velocity fluctuations were measured with an X-film anemometer (Thermal Systems, Inc.). The two cross channels were converted to horizontal and vertical velocity components using an iterative routine based on King's law. The X-film, along with Pitot and Elliott pressure probes, were mounted on the "wind profiler", an instrumented support structure designed to move 4 m along a track parallel to, and 2.5 m outboard of, the northeast leg of the tower (41 cm dia). The profiler, 2.5 m in height, was vaned so that it would point into the wind, and positioned relative to the surface by computer control from shore. Further details on the profiler, and on the operation and calibration of the X-film and pressure probes, are available in Donelan *et al.* (1999).

The surface elevation was measured using capacitance waves gauges. The directional distribution of the wave field was determined using maximum likelihood analysis (Capon 1969) on the signals from an array of six gauges forming a centered pentagon of 25 cm radius. The near surface current was measured at two depths, roughly 0.5 and 2m, using drag sphere current meters (Donelan and Motycka 1978).

### 3. Analysis

The WAVES87 campaign took place during the eight week period between late October and mid December 1987. During this period, 306 flux runs of 30-min were gathered. Meteorological conditions during these runs are summarised in Figure 3. During the autumn, the area is dominated by three types of events. The prevailing winds are SW, and winds from this direction clockwise through north result in fetch limited conditions with inverse wave ages ( $U_\theta/c_p$ ) typically around 3 - 5. Here  $c_p$  is the phase velocity of waves at the peak of the spectrum, and  $U_\theta$  the component of the wind in peak direction of the waves (Donelan *et al.* 1985). Below, we denote the inverse wave age as  $U/c_p$ . Significant wave heights range from well under 0.5 m for pure

wind sea conditions to over 2 m in the case of counter swells propagating down the lake. Winds from the east yield waves of order 1 m, with inverse wave ages from near zero to 2. In these cases, it is often difficult to discern the active wind sea component of the spectrum, especially if the wind is decaying. Finally, there are a significant number of cases of NNE winds. In these cases, the wind sea is typically accompanied by waves propagating down the lake, from the direction of the longest fetch, roughly ENE (Donelan *et al.* 1985).

The 306 runs were initially examined based on several criteria. Runs with mean wind speeds below  $3.5 \text{ ms}^{-1}$  or any 1-min average wind speed below  $2 \text{ ms}^{-1}$  were rejected on the grounds that the bivariate is not expected to perform well in these conditions. Also, runs that exhibited large changes in either wind speed or wind direction were rejected as being nonstationary. Data were screened for spikes. These criteria together eliminated 57 runs from the data set. In carrying out the eddy-correlation stress calculations, the time series were first detrended, but no filtering was carried out.

Over water, where the roughness is not directionally homogeneous, the stress is given by

$$\tau = \rho(-\overline{u'w'i} - \overline{v'w'j}). \quad (6)$$

Here,  $u'$ ,  $v'$  and  $w'$  are the turbulent components of horizontal in-line (with the mean wind), horizontal cross, and vertical air velocities respectively. For brevity, we henceforth omit the primes from the notation. (6) differs from (1) in accounting for contributions to the stress which are not aligned with the mean wind (Geernaert *et al.* 1993). The near surface currents were calculated from velocity data from the drag sphere current meters. For most runs, the upper current meter, at approximately 0.5 m depth was used. However, under high wave conditions, this instrument was covered to avoid damage; the lower current meter (2m) was used in these circumstances. For each run, the drag spheres were oriented into the dominant waves to yield along-wave and vertical current

components. During the WAVES87 campaign, along-wave mean currents are of  $O(0.1 \text{ ms}^{-1})$

Drag coefficients, both 12m and 10m-neutral, are calculated from the data. In determining the Monin-Obukhov length (2), an iterative routine is used.  $u_*$  is the measured friction velocity, while the heat and moisture fluxes are determined from bulk relations, using measured mean values of temperature and humidity, and assuming Dalton and Stanton numbers of 0.0012 (Large and Pond, 1981).

The runs are classified according to wave conditions. Peak frequencies of both the full spectrum and wind sea (if different) were found, and  $c_p$  and the wave age were calculated. Note that, in general, swells observed at the tower tend to come from the direction of longest fetch, about 70 deg, ENE (Donelan *et al.* 1985). Based on the directional spectra, seven categories were used: i) pure wind sea, short fetch; ii) pure wind sea, long fetch; iii) wind sea (NNE) with long fetch waves propagating from the ENE; iv) short fetch with dominant counterswell; v) short fetch with nondominant counterswell; vi) short fetch winds (NW or S) with cross swells; and vii) wind sea (E) with following swells.

For comparison, we include open ocean data collected from a small ship during the SWADE experiment (Donelan *et al.* 1997). These are eddy correlation data from a K-Gill anemometer mounted on a mast near the bow, with full motion correction carried out using the measured six degrees of ship motion. Directional wave spectra were obtained from the ship, using an array of wave staffs, again taking into account the motion of the ship.

#### 4. Pure wind sea data

In Fig. 4 we plot 12 m non-neutral drag coefficients versus wind speed for the full data set. The large degree of scatter is typical of such plots, and points to the likelihood that variables other than wind speed are important in parameterising  $C_D$ . These data, and all data discussed below, are from the 12m bivariate, unless otherwise specified. As a

starting point to further analysis, we restrict attention to cases of pure wind sea. This eliminates possible variability due to the presence of background swells (Geernaert *et al.* 1986; Donelan *et al.* 1997; Rieder 1997). The wind sea data, 107 runs, are denoted by circles in Fig. 4, with the short- and long-fetch data denoted by hollow and filled circles respectively. The scatter is not significantly reduced from the full data set, but a strong stratification between the short-fetch,  $O(1 \text{ km})$  and long-fetch,  $O(100 \text{ km})$ , data is evident. This is the wave age effect reported by Donelan (1990), Smith *et al.* (1992) and others. The short fetch data are primarily young wind sea, mostly with  $2.5 < U/c_p < 4.5$ , while the long fetch data represent more mature seas, with inverse wave ages around 1 to 2 (Table 1).

$U/c_p$	long fetch	short fetch	SWADE
0.8 – 1.5	27	5	15
1.5 – 2.5	11	9	8
2.5 – 3.5	0	33	0
3.5 – 4.5	0	22	0

Table 1. Pure wind sea runs classified by inverse wave age,  $U/c_p$ . Data are WAVES-long fetch, WAVES-short fetch, and SWADE, Donelan *et al.* 1997.

An alternative means of showing this is via the roughness length,  $z_o$ , which is related to the drag coefficient as discussed above. Calculating the dimensionless surface roughness, that is the ratio of  $z_o$  to  $\sigma$ , the standard deviation of the wave height, we see in Figure 5 that  $z_o/\sigma$  increases with inverse wave age as measured by  $u_*/c_p$ . Younger waves are rougher, and the drag coefficient over them is commensurately higher. The pure windsea data set is in very good agreement with the Donelan (1990) curve, which was established at the same site, but with data gathered in a different year, viz. 1976. The SWADE open ocean data, with wave ages similar to the long fetch data (Table 1) are also seen to support the curve.

If we now focus on the mature pure wind sea data, long fetch plus SWADE, we find the scatter of  $C_D$  versus  $U$  much reduced ( $r = 0.73$ , versus  $r = 0.41$  for all WAVES data). In Fig. 6, the long-fetch and SWADE wind sea 10 m neutral drag coefficients are plotted. The two data sets are in very good agreement, and a regression to them yields  $1000C_{D10N} = 0.117U_{10N} + 0.15$ , with a correlation coefficient of 0.8. For comparison, the curve of Yelland and Taylor (1996) is plotted: clearly the low wind speed behaviour of the Yelland and Taylor data is not observed here.

A consequence of Monin-Obukhov similarity theory is that, in some wavenumber range, we expect the velocity spectra to follow some universal shape when scaled in the appropriate manner (Busch 1973). Considerable effort has been spent in determining the universal forms, and there are several alternative formulations. Kaimal *et al.* (1972), using data profiles from the 1968 Kansas experiment, normalised the velocity spectra by spectral energy in the inertial subrange. Their classic results indicate strong support for universal spectral shapes, with the dimensionless spectra being functions of dimensionless frequency,  $fz/U$ , and stability,  $z/L$ . The spectra of Miyake *et al.* (1970), based on near-neutral data over the coastal sea, demonstrate similar universality over the ocean. Other marine data sets, e.g. Smith and Anderson (1984), support the proposed curves.

In Fig. 7, we plot universal  $S_{ww}$ ,  $S_{uu}$  and  $S_{uw}$  spectra, calculated from the pure wind sea data (all wave ages), using the scaling of Miyake *et al.* (1970). The curves of Miyake *et al.*, derived from visual fits to their plots, are also shown (dashed). For  $S_{ww}$  and  $S_{uw}$ , the Miyake curves fall within one standard error (shaded area) of the WAVES87 universal curve except at high frequency, where the Miyake *et al.* curves depart from the expected inertial subrange behaviour (due to limited anemometer response – Kaimal *et al.* 1972). For the horizontal velocity spectrum  $S_{uu}$ , the WAVES87 universal curve is higher than that of Miyake *et al.* by nearly a factor of two at lower frequencies, likely due to different mesoscale behaviour at the two sites. For the WAVES87 data

$\sigma_u/\sigma_w = 2.8 \pm 0.5$  (showing 1 standard deviation), compared to  $1.9 \pm 0.2$  for the Miyake *et al.* data.

Run	Time JD	length min	$U$ $\text{ms}^{-1}$	$-\overline{uw}$ $\text{m}^2\text{s}^{-2}$	$-\overline{vw}$ $\text{m}^2\text{s}^{-2}$	$u_*^2\text{-ID}$ $\text{m}^2\text{s}^{-2}$	$\sigma_w$ $\text{ms}^{-1}$	$\sigma_w/U$	$T_a$ $^{\circ}\text{C}$	$T_w$ $^{\circ}\text{C}$	$H_s$ m	$f_p$ Hz	$U/c_p$	Symbol
a) Pure wind sea runs														
87128	331.55	90	9.60	0.112	-0.003	0.100	0.38	0.039	2.24	4.52	1.45	0.18	1.15	o
"	"	"	8.14	0.121		0.073	0.28	0.034	Hotfilm at 2.1m					*
87176	344.79	90	4.70	0.019	-0.003	0.025	0.22	0.046	5.44	4.20	0.10	0.85	2.47	x
b) Swell runs, low wind speed														
87056	319.85	90	4.30	0.017	-0.002	0.028	0.14	0.033	7.03	6.85	0.67	0.22	0.61	◇
87144	333.33	90	4.76	-0.006	-0.004	0.028	0.19	0.040	5.00	4.13	1.45	0.16	0.48	▷
87145	333.41	90	4.92	-0.001	-0.004	0.032	0.17	0.034	4.83	4.20	1.44	0.16	0.44	*
87146	333.64	90	3.90	-0.012	0.003	0.006	0.09	0.024	5.51	4.30	1.17	0.16	0.44	●
87147	333.72	60	4.27	-0.001	-0.001	0.019	0.13	0.030	5.18	4.33	1.11	0.16	0.47	o
c) Swell runs, moderate wind speed														
87117	330.01	60	7.49	0.018	-0.009	0.053	0.26	0.035	2.88	4.96	2.53	0.13	0.74	x
87119	330.26	90	7.57	0.059	0.039	0.064	0.31	0.041	0.09	4.88	1.46	0.14	0.60	*
87120	330.39	60	8.01	0.078	0.055	0.074	0.35	0.043	0.13	4.75	1.27	0.15	0.63	o

Table 2: Summary of WAVES87 data highlighted in the text.  $U$  is the mean wind speed, and  $u$ ,  $v$  and  $w$  are the turbulent components of horizontal in-line (with the mean wind), horizontal cross, and vertical air velocities respectively.  $u_*^2\text{-ID}$  is the square of the friction velocity calculated via the inertial dissipation method of Large and Pond 1981, and  $\sigma_w$  is the standard deviation of  $w$ .  $T_a$ ,  $T_w$  and  $H_s$  are the mean air and water temperatures, and the significant wave height, respectively.  $f_p$  and  $c_p$  are the frequency of the peak of the surface wave spectrum, and the corresponding phase velocity. Unless otherwise specified, data are from a bivanne at 12m. The symbols in parts (a), (b) and (c) refer to Figures 8, 11-14, and 15 respectively.

The data are also categorised by stability, and the spectra in four stability ranges are shown. There is little evidence for a departure from the single universal curve based on stability. Only the most stable data (circles) show departure from the universal behaviour, but with only 4 runs, the significance is low. In Fig. 8, we plot typical spectra from two 90-min runs: one with light-moderate 12m winds ( $4.7 \text{ ms}^{-1}$ ) and short-fetch waves ( $U/c_p = 2.47$ ;  $H_s = 0.1\text{m}$ ); the other with stronger 12m winds ( $9.6 \text{ ms}^{-1}$ ) and long-fetch waves ( $U/c_p = 1.15$ ;  $H_s = 1.4\text{m}$ ) – see Table 2a. The plot shows scatter around the universal curve typical of the pure wind sea data: in general there is very good agreement. In addition to the 12m bivariate data, data from the X-film anemometer at 2.1 m are shown for the long fetch case ( $H_s = 1.4 \text{ m}$ ). Again, these data are seen to support the universal curve. This is consistent with the estimates of Janssen (1989) and Makin and Mastenbroek (1996) as discussed above, and shows strong support for the validity of MO similarity over pure wind seas over a wide range of wave age.

## 5. Stress data: Mixed wind sea and swell

The stress angle has been shown to deviate significantly from the wind direction in some situations, and this has been attributed, at least in part, to the effect of swells (Geernaert *et al.* 1993; Rieder *et al.* 1994). In Figure 9, we plot the relative angle of the stress vector to the mean wind ( $u$ ) direction,  $\arctan(\overline{vw}/\overline{uw})$ . When swell is present, particularly at low wind speeds, there is often a considerable difference between the wind and stress directions. For the pure wind sea data, the mean stress direction is generally in line with the wind.

In studying the effects of swell on the stress, we focus on the long-fetch data so as to remove the additional effect of wave age. In Fig. 10 the long-fetch WAVES data are plotted, classified as either pure wind sea or wind sea with following swell. For contrast, a subset of the SWADE data (Donelan *et al.* 1997) are also plotted: the pure wind sea cases and the cases of wind sea with counter swell. Whereas the SWADE *counter-swell* runs were observed to result in *enhanced stress*, the following swell cases here are

seen to be associated with a distinct decrease in stress. These data include cases where the stress is near-zero, and sometimes negative (i.e upward). Hence, the WAVES data provide strong support for a dependence of stress on swell properties.

In Figure 11 horizontal and vertical velocity spectra from the bivariate, and the surface wave height spectrum are plotted for a typical diminished or upward flux case (run 87146 – see Table 2b). These are runs with ‘fast’ swells,  $U/c_p \approx 0.45$ , travelling in roughly the same direction as the wind. At the bivariate height of 12 m, the signature of the swell ( $H_s = 1.2\text{m}$ ) is clearly evident in the wind velocity spectra.

In Figure 12 are plotted spectra of bivariate vertical and horizontal (in-line) velocity for following swell cases, along with the universal curve derived from the pure wind sea data. For the purposes of comparison on the dimensional plot, the data are restricted to following swell in the mean wind speed range,  $U \approx 3.9 - 4.9\text{ms}^{-1}$ . The data are outlined in Table 2b. Typically,  $U/c_p \approx 0.45$  and  $H_s\text{-swell} \gg H_s\text{-windsea}$ : these are examples of fast, strong swell. As is expected, the data stratify to some extent by wind speed: the filled and hollow circles represent the lowest and next-lowest wind speed runs respectively. The universal curve is rendered dimensional using the values from a pure wind sea run in the same wind speed range (run 87176, Table 2a). In Fig. 12 it is clear that while turbulence levels in the inertial subrange follow the pure wind sea data quite well, there is considerable departure at lower frequencies, most notably at frequencies lower than that of the swell waves where the turbulence levels are reduced by up to an order of magnitude over pure wind sea values.

In Figure 13, the same data are plotted, this time in the universal coordinates of Miyake *et al.* (1970). Here,  $\sigma_w$  is determined from the turbulent velocity components alone, i.e. excluding the wave-coherent component. It is evident that spectral similarity does not hold when the swells are present. The inertial subrange values are consistently higher than those of the pure wind sea cases, while the pure wind sea curves overestimate the energy at low frequencies. If on the other hand, the spectra are scaled on the

inertial subrange values (c.f. Kaimal *et al.* 1972) it is clear that the low frequency behaviour exhibits significant (order of magnitude) departure from the universal curves.

In Figure 14, the  $uw$  cospectra for the same runs are shown. Recalling that  $z$  and  $U$  are similar for all runs, it is clear that there is generally substantial departure from the universal cospectrum established earlier. In particular at low frequencies, those below that of the swell, the stress is greatly reduced, or even upward. This reduction in stress is consistent with the general reduction in turbulent energy at these frequencies, as noted above. Reidner and Smith (1998), in their study of the effects of swell on the stress vector, concluded that the major effects of swell on stress were contained in the mid-range of frequencies, roughly 0.06-0.16 Hz. Our results do not support this, but indicate an effect at all frequencies lower than that of the swell.

The behaviour described above is least evident with run 87056 (designated by  $\diamond$  in Figs. 12-14). This run differs from the remaining fast swell runs in several ways: The inverse wave age is higher than that of the other cases (0.61 versus 0.44-0.48) and the swell energy is lower by roughly a factor of two. Also, the swell peak frequency is higher. Designating the peak wavenumber of the swell by  $k_p$ ,  $\exp(-2k_p z) = 0.009$  at 12m for run 87056, versus 0.06 for the remaining runs. Given that the influence of the waves on the atmospheric turbulence spectra is expected to decrease with height as  $\exp(-2k_p z)$  (Makin and Mastenbroek, 1996), each of these factors would reduce the observed effect.

Finally, we present data typical of slower swell cases, those with  $U/c_p \approx 0.7$ . Due to the fetch geometry of the lake (Fig. 2), there is generally little variation in the swell frequency. Hence slow swells are those coexisting with higher velocity winds. Here the swell is the result of a decrease in wind speed (from  $13 \text{ ms}^{-1}$  to  $7 \text{ ms}^{-1}$ ) and a  $40^\circ$  shift in wind direction which took place just prior to the first run. The resulting directional wave spectra are bimodal, with dominant swell peaks. The velocity spectra and cospectra are plotted along with the pure wind sea curves in Fig. 15. The data are described in Table 2c. Although there is some scatter, in general the data are in

agreement with the universal curves, with the exception of  $S_{uw}$  for run 87117. Here, although the shape of the curve appears consistent with the universal curve, there are significant positive stress contributions at low frequencies. These contributions, perhaps associated with a 20° wind shift, which occurred during the run, lead to a decreased  $u_*$ , and hence the positive offset of the curve. In general though, the slow swell cases are consistent with the pure wind sea data. This might be anticipated from Fig. 10 in that there is no distinction in drag between the pure wind sea and following swell cases at these wind speeds.

## 6. Discussion

We have presented evidence that swell effects can be felt at a considerable height above the surface. Velocity spectra and cospectra measured over pure wind sea, with waves of a wide range of development ( $U/c_p \approx 0.8 - 4.5$ ), agreed with the universal curves of Miyake *et al.* (1970). Furthermore measured wind velocities and spectra at heights as low as 2 m ( $H_s = 1.4$ m) showed no evidence of significant wave-coherent components. This is consistent with the estimates of Janssen (1989) and Makin and Mastenbroek (1996), and implies that turbulent stress dominates the total stress at typical measurement heights over pure wind seas. Likewise, turbulent spectra taken over slower swells ( $U/c_p \approx 0.7$ ) agreed with the universal curves. Hence Monin-Obukhov similarity theory is expected to perform well in these conditions. In contrast, with fast, strong swells present ( $U/c_p \approx 0.5$ ,  $H_{s\text{-swell}} \gg H_{s\text{-windsea}}$ ) wave effects were evident in the wind velocity spectra at heights of 12 m, with  $H_s \approx 1.2$ m. Turbulence levels were significantly reduced over pure wind sea values, and significant deviations from the universal spectral shapes were found. Consequently, we do not expect MO theory to be valid in these conditions.

Smedman *et al.* (1994) recorded fluxes and profiles from aircraft and a nearshore tower, and observed several events in which a light onshore wind was blowing shortly after the passage of a storm. Although they had no supporting wave data, it was

assumed that conditions were similar to those observed here, with swell propagating onshore. Their observed profiles indicated nearly constant wind speed with height, consistent with their estimations of very low surface stress ( $C_D \approx 0.5 \times 10^{-3}$ ). They interpreted the observations as ‘shearfree’ turbulence, with no active shear production at the air-sea boundary. Instead, pressure transport was found to be significant in carrying turbulent energy produced at higher elevations by shear down to the surface layer. Such a mechanism would explain the apparent paradox observed in the present data: that the high turbulent energy levels in the inertial subrange are apparently not supported by the classical cascade of turbulent energy from longer scales. Although such high level pressure measurements were not made during the WAVES campaign, near surface measurements show an upward pressure transport from the swell to the atmosphere during fast following swell conditions (Kahma *et al.* 1999). Hence pressure transport is likely important in the presence of swell.

As was pointed out by Smedman *et al.* (1994),  $u_*$  is no longer a valid scaling variable when the stress is near zero (or negative). Given that measured stress is near-zero in conditions of strong following swell, it is perhaps not surprising that velocity spectra and cospectra do not follow MO scaling under these conditions. There are significant consequences arising from this. First of all, the use of MO based stability relations for transforming measured stress values to neutral 10 m values should be re-examined for use over the ocean. Secondly, the commonly used inertial dissipation (ID) method for estimating fluxes must also be called into question in use over the open ocean. The method is derived from the turbulent kinetic energy (TKE) conservation equation

$$u_*^2 \frac{\partial U}{\partial z} + g \frac{(\overline{w\theta} + 0.61 T_o \overline{wq})}{T_o} - \epsilon - \frac{\partial \overline{we}}{\partial z} - \frac{\partial \overline{wp}}{\partial z} = 0 \quad (7)$$

where  $e$  and  $p$  are fluctuations in turbulent kinetic energy and pressure respectively. The terms are, respectively, production of TKE from shear, production (or loss) due to

buoyancy, loss due to dissipation, transport of TKE and pressure transport. Dividing (7) by  $u_*^3/\kappa z$ , we arrive at

$$\phi_u - \zeta - \frac{\kappa z}{u_*^3} \epsilon - \phi_t = 0 \quad (8)$$

where  $\phi_t$  represents the combined transport terms. Following MO theory,  $\phi_u$  and  $\phi_t$  are expected to be universal functions of  $\zeta$ , although it is often assumed that  $\phi_t = 0$  (Large and Pond, 1981). Then from a known dissipation rate (usually estimated from the inertial subrange of the frequency spectrum, assuming Taylor's hypothesis), and known dimensionless functions (e.g. those of Höglström, 1996), the stress can be readily determined.

The method has gained considerable popularity because it relies only on the high frequency velocity components, which are not as susceptible to platform motion or flow distortion. Consequently the method is often used from ships at sea (Large and Pond 1981; Yelland and Taylor 1996). Studies comparing momentum fluxes determined by the eddy-correlation (EC) and ID methods have typically reported good agreement, with rms differences of approximately 20% (Large and Pond 1981; Edson *et al.* 1991). Donelan *et al.* (1997) found similar agreement for their pure wind sea data, but found a doubling of the rms difference in their comparison when swells were present. When fast, strong opposing swells were present, the EC fluxes were approximately double the ID fluxes.

However,  $\phi_u$  can not be assumed to be a function of  $\zeta$  alone in the event that the assumptions of MO theory are violated. Hence on the basis of this work, ID theory can not be expected to work in the presence of fast swells. This is evident in the fast swell data of Table 2b: Whereas the eddy correlation data exhibit very low stress, the inertial dissipation stress values differ little from the pure wind sea values (e.g. run 87176). As seen in Figure 12, turbulence levels in the inertial subrange are similar for pure wind sea and swell runs of similar wind speed; turbulence levels at the lower frequencies

are however significantly different. When spectra do not follow universal scaling, high frequency behaviour is no longer a good surrogate for the overall spectrum.

It is interesting to note that of the previous work on the effects of swell on momentum flux, the studies reporting no significant effect were based on inertial dissipation data (Dobson *et al.* 1994; Yelland and Taylor 1996). On the other hand an effect was reported in the eddy correlation studies. In the context of the above, it is not surprising that this should be the case. It is now clear that the inertial dissipation method itself is invalid in these conditions.

## 7. Conclusions

- 1) The momentum flux can be strongly affected, even to the extent of changing direction, by the presence of swell. Hence, any relationship between  $C_D$  and  $U$  must take this variable into account.
- 2) In pure wind sea conditions spectra follow universal scaling, hence Monin-Obukhov similarity theory would appear to hold [at typical measurement heights]. This is consistent with WBL height estimates of Janssen (1969) and Makin and Mastenbroek (1996), and measurements of Edson and Fairall (1998).
- 3) In the presence of fast swells, turbulent velocity spectra and cospectra do not follow Monin-Obukhov scaling. In particular, turbulence is dramatically reduced at frequencies about and lower than that of the following swell.
- 4) The inertial dissipation method of estimating fluxes is not expected to be valid in the presence of fast swells travelling either with (this paper) or against (Donelan *et al.* 1997) the wind.
- 5) The standard practice of transforming meteorological data to neutral conditions is invalid in the presence of fast swells.

In midlatitudes, such fast swells are often associated with frontal passages, or may occur following a storm. In the tropics, where the winds are weaker, such conditions

often occur in advance of, or following, the passage of tropical storms. Hence the results have particular significance in accurate modelling of extreme events.

For many years, campaigns to determine the drag coefficient over the sea have been carried out. Yet the experimental scatter in the data, both within and between experiments, remains large, especially at low wind speeds. The results here suggest that this is due, at least in part, to the presence of swells. Other conditions, such as rapidly turning winds, are also likely factors (Rieder 1997). In order for bulk formulations to successfully reflect these factors, Monin-Obukhov similarity theory must be extended to include additional variables. This study suggests that the swell related variables  $U/c_p$ ,  $k_p z$  and  $H_s\text{-swell}/H_s\text{-windsea}$  are good candidates, although clearly further work is required to quantify the effects.

#### *Acknowledgements.*

WD and KK thank the staff of the National Water Research Institute, Burlington for their hospitality during their respective post-doctoral periods and during their many subsequent visits. We gratefully acknowledge the contribution of many members of the engineering and technical staff of NWRI in the design, construction and operation of the apparatus; in particular: D. Beesley, Y. Desjardins, R. Desrosiers, N. Madsen, M. Pedrosa, H. Savile and J. Valdmanis. WD and MD acknowledge partial ONR support for the analysis work, through grant N00014-97-1-0015.

## REFERENCES

- Busch, N.E.: 1973, 'On the mechanics of atmospheric turbulence', In: *Workshop on micrometeorology*, (D.A. Haugen, Ed.), Am. Meteorol. Soc., 1-65.
- Businger, J.A., J.C. Wyngaard, Y.K. Izumi and E.F. Bradley: 1971, 'Flux-profile relationships in the atmosphere surface layer', *J. Atmos. Sci.* **28**, 181-189.
- Capon, J.: 1969, 'High-resolution frequency-wavenumber spectrum analysis', *Proc. IEEE* **57**, 1408-1418.
- Charnock, H.: 1955, 'Wind stress on a water surface', *Quart. J. Roy. Meteorol. Soc.* **81**, 639-640.
- Dobson, F.W., S.D. Smith and R.J. Anderson: 1994, 'Measuring the relationship between wind stress and sea state in the open ocean in the presence of swell', *Atmos. Ocean* **32**, 237-256.
- Donelan, M.A.: 1990, 'Air-Sea Interaction', In: *The Sea: Ocean Engineering Science*, **9**, (B. LeMéhauté and D. Hanes, Eds.), John Wiley and Sons, Inc., New York, 239-292.
- Donelan, M.A., K.N. Birch and D.C. Beesley: 1974, 'Generalized profiles of wind speed, temperature and humidity', In: *Proc. 17th conf. Great Lakes Res.* 369-388.
- Donelan, M.A., F.W. Dobson, S.D. Smith and R.J. Anderson: 1993, 'On the dependence of sea surface roughness on wave development', *J. Phys. Oceanogr.*, **23**, 2143-2149.
- Donelan, M.A., W.M. Drennan and K.B. Katsaros: 1997, 'The air-sea momentum flux in mixed wind sea and swell conditions', *J. Phys. Oceanogr.* **27**, 2087-2099.
- Donelan, M.A., J. Hamilton and W.H. Hui: 1985, 'Directional spectra of wind generated waves', *Phil. Trans. R. Soc. London* **A315**, 509-562.
- Donelan, M.A., N. Madsen, K.K. Kahma, I.K. Tsanis and W.M. Drennan: 1999, 'Apparatus for atmospheric boundary layer measurements over waves', *J. Atmos. Oceanic Technol.* [in press]
- Donelan, M.A., and J. Motyka, 1978: 'Miniature drag sphere velocity probe', *Rev. Sci. Instrum.* **49**, 298-304.

- Drennan, W.M., H.C. Graber and M.A. Donelan: 1999, 'Evidence for the effects of swell and unsteady winds on marine wind stress', *J. Phys. Oceanogr.* [in press]
- Dyer, A.J, and B.B. Hicks: 1970, 'Flux-gradient relationships in the constant flux layer', *Quart. J. Roy. Meteorol. Soc.* **96**, 715-721.
- Edson, J.B., and C.W. Fairall: 1998, 'Similarity relationships in the marine atmospheric surface layer for terms in the TKE and scalar variance budgets', *J. Atmos. Sci.* **55**, 2311-2328.
- Edson, J.B., C.W. Fairall, P.G. Mestayer and S.E. Larsen: 1991, 'A study of the inertial-dissipation method for computing air-sea fluxes', *J. Geophys. Res.* **96**, 10689-10711.
- Geernaert, G.L., F. Hansen, M. Courtney and T. Herbers: 1993, 'Directional attributes of the ocean surface wind stress vector', *J. Geophys. Res.* **98**, 16571-16582.
- Geernaert, G.L., K.B. Katsaros and K. Richter: 1986, 'Variations of the drag coefficient and its dependence on sea state', *J. Geophys. Res.* **91**, 7667-7679.
- Hicks, B.B.: 1972, 'Propeller anemometers as sensors of atmospheric turbulence', *Boundary-Layer Meteorol.* **3**, 214-228.
- Högström, U.: 1996, 'Review of some basic characteristics of the atmospheric surface layer', *Boundary-Layer Meteorol.* **78**, 215-246.
- Holland, J.Z., W. Chen, J.A. Almazam and F.C. Elder: 1981, 'Atmospheric boundary layer', In: *IFYGL - The international field year for the Great Lakes*, Eds: E.J. Aubert and T.L. Richards, NOAA, Ann Arbor, 109-167.
- Janssen, P.A.E.M.: 1989, 'Wave-induced stress and the drag of air flow over sea waves', *J. Phys. Oceanogr.* **19**, 745-754.
- Kahma, K.K., M.A. Donelan and W.M. Drennan: 1999, 'Energy flux from swell to wind: evidence from pressure fluctuation measurements', [in preparation].
- Kaimal, J.C., J.C. Wyngaard, Y. Izumi and O.R. Coté: 1972, 'Spectral characteristics of surface-layer turbulence', *Quart. J. R. Met. Soc.*, **98**, 563-589.

- Kitaigorodskii, S.A., and Y.A. Volkov: 1965, 'On the roughness parameter of the sea surface and the calculation of momentum flux in the near-water layer of the atmosphere', *Izv., Atmos. and Oceanic Phys.* **1**, 973-988.
- Large, W.G. and S. Pond: 1981, 'Open ocean momentum flux measurements in moderate to strong winds', *J. Phys. Oceanogr.* **11**, 324-336.
- MacCready, P.B., and H.R. Jex: 1964, 'Response characteristics and meteorological utilization of propeller and vane wind sensors', *J. Appl. Meteor.* **3**, 182-193.
- Makin, V.K., and C.Mastenbroek: 1996, 'Impact of waves on air-sea exchange of sensible heat and momentum', *Boundary-Layer Meteorol.* **79**, 279-300.
- Miyake, M., R.W. Stewart and R.W. Burling: 1970, 'Spectra and cospectra of turbulence over water', *Quart. J. Roy. Meteor. Soc.* **96**, 138-143.
- Monin, A.S., and A.M. Obukhov: 1954, 'Basic laws of turbulent mixing in the ground layer of the atmosphere', *Akad. Nauk. SSSR Geofiz.Inst. Tr.* **151**, 163-187.
- Obukhov, A.M.: 1946, 'Turbulence in an atmosphere with a non-uniform temperature', *Boundary-Layer Meteorol.* **2**, 7-29, 1971.
- Rieder, K.F.: 1997, 'Analysis of sea-surface drag parameterizations in open ocean conditions', *Boundary-Layer Meteorol.* **82**, 355-377.
- Rieder, K.F., and J.A. Smith, 1998: Removing wave effects from the wind stress vector. *J. Geophys. Res.* **103**, 1363-1374.
- Rieder, K.F., J.A. Smith and R.A. Weller: 1994, 'Observed directional characteristics of the wind, wind stress and surface waves on the open ocean', *J. Geophys. Res.* **99**, 22589-22596.
- Smedman, A.S., U. Högström, H. Bergström, A. Rutgersson, K.K. Kahma and H. Pettersson: 1999, 'A case study of air-sea interaction during swell conditions', Submitted to *J. Geophys. Res.*

- Smedman, A.S., M. Tjernström, and U. Högström: 1994, 'The near-neutral marine atmospheric boundary layer with no surface shearing stress: a case study', *J. Atmos. Sci.* **51**, 3399-3411.
- Smith, S.D.: 1980, 'Wind stress and heat flux over the ocean in gale force winds', *J. Phys. Oceanogr.* **10**, 709-726.
- Smith, S.D., and R.J. Anderson, 1984: 'Spectra of humidity, temperature and wind over the sea at Sable Island, Nova Scotia', *J. Geophys. Res.* **89**, 2029-2040.
- Smith, S.D., R.J. Anderson, W.A. Oost, C. Kraan, N. Maat, J. deCosmo, K.B. Katsaros, K.L. Davidson, K. Bumke, L. Hasse and H.M. Chadwick: 1992, 'Sea surface wind stress and drag coefficients: the HEXOS results', *Boundary-Layer Meteorol.* **60**, 109-142.
- Smith, S.D., C.W. Fairall, G.L. Geernaert and L. Hasse: 1996, 'Air-sea fluxes: 25 years of progress', *Bound. Layer Meteorol.* **78**, 247-290.
- Stewart, R.W.: 1961, 'The wave drag of wind over water', *J. Fluid Mech.* **10**, 189-194.
- Terray, E.A., M.A. Donelan, Y.C. Agrawal, W.M. Drennan, K.K. Kahma, A.J. Williams III, P.A. Hwang and S.A. Kitaigorodskii: 1996, 'Estimates of kinetic energy dissipation under breaking waves', *J. Phys. Oceanogr.* **26**, 792-807.
- Yaglom, A.M.: 1977, 'Comments on wind and temperature flux-profile relations', *Boundary-Layer Meteorol.* **11**, 89-102.
- Yelland, M.J., and P.K. Taylor: 1996, 'Wind stress measurements from the open ocean', *J. Phys. Oceanogr.* **26**, 541-558.
- Zilitinkevich, S.S., and D.V. Chalikov: 1968, 'Determining the universal wind velocity and temperature profiles in the atmospheric boundary layer', *Izv., Atmos. and Oceanic Phys.* **4**, 165-170.

FIG. 8. Representative wind sea data in the universal scaling of Miyake *et al.* (1970). The panels show spectra of vertical velocity (a) and cospectra between the vertical and horizontal in-line velocity (b). The data represented by  $\circ$  and  $\times$  are from the 12 m bivariate with wind speed  $U = 9.6$  and  $4.7\text{ms}^{-1}$  respectively. The  $*$  data are from a hotfilm at 2.1m, during the same run as the  $\circ$  data – see Table 2a. The shaded area denotes  $\pm 1$  standard error from the mean curve established from all wind sea data.

FIG. 9. Stress offwind angle with respect to the mean wind direction vs. 12 m wind speed. Pure wind sea ( $\circ$ ); mixed seas ( $\times$ ).

FIG. 10. 12 m non-neutral data from WAVES (pure wind sea,  $\bullet$ , and following swell,  $\times$ ) and SWADE (Donelan *et al.* 1997: pure wind sea,  $*$ , and counter swell,  $\diamond$ ).

FIG. 11. Spectra from run 87146, with light winds and fast following swell. Curves are downwind ( $\times 10$ ) and vertical velocity spectra from bivariate at 11.9m and surface elevation spectrum.  $U = 3.9\text{ms}^{-1}$ ,  $H_s = 1.2\text{m}$ , and  $U/c_p = 0.44$ .

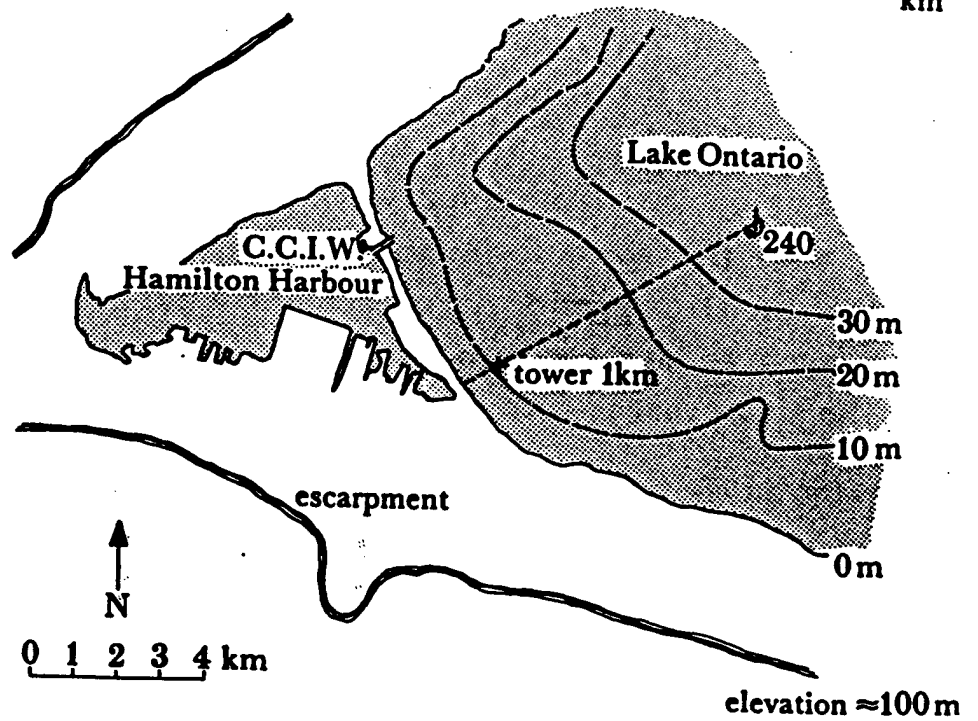
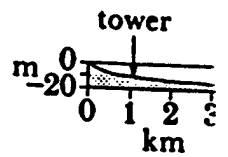
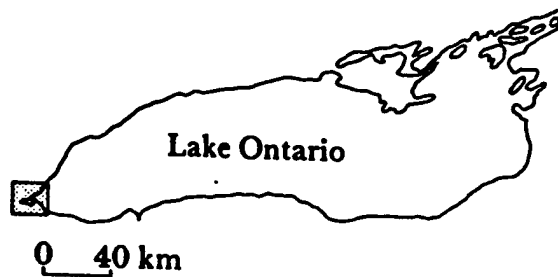
FIG. 12. Spectra of vertical (a) and horizontal in-line (b) velocity during swell runs. The data, described in Table 2b, are from the wind speed range  $U \approx 4 - 5\text{ms}^{-1}$ . For the  $\diamond$  data,  $U/c_p = 0.61$ ; for the other data,  $U/c_p < 0.5$ . The solid line is the pure wind sea universal curve, rendered dimensional using the data of pure wind sea run 87176.

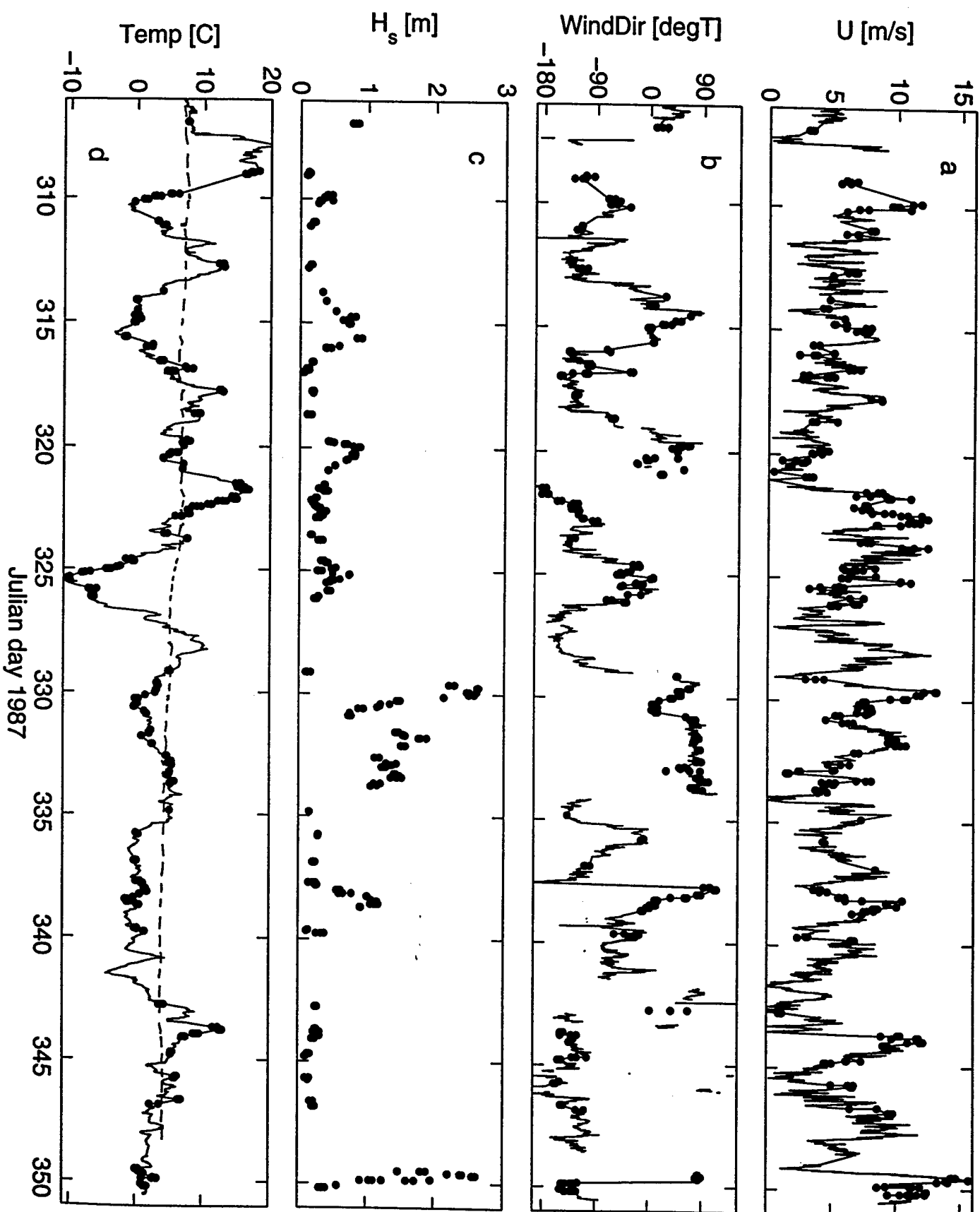
FIG. 13. Spectra of vertical (a) and horizontal in-line (b) velocity from swell runs, plotted in the universal scaling of Miyake *et al.* (1970). The data, described in Table 2b, are from the wind speed range  $U \approx 4 - 5\text{ms}^{-1}$ . For the  $\diamond$  data,  $U/c_p = 0.61$ ; for the other data,  $U/c_p < 0.5$ . The shaded areas represent  $\pm$  one standard error about universal curves established from the pure wind sea data.

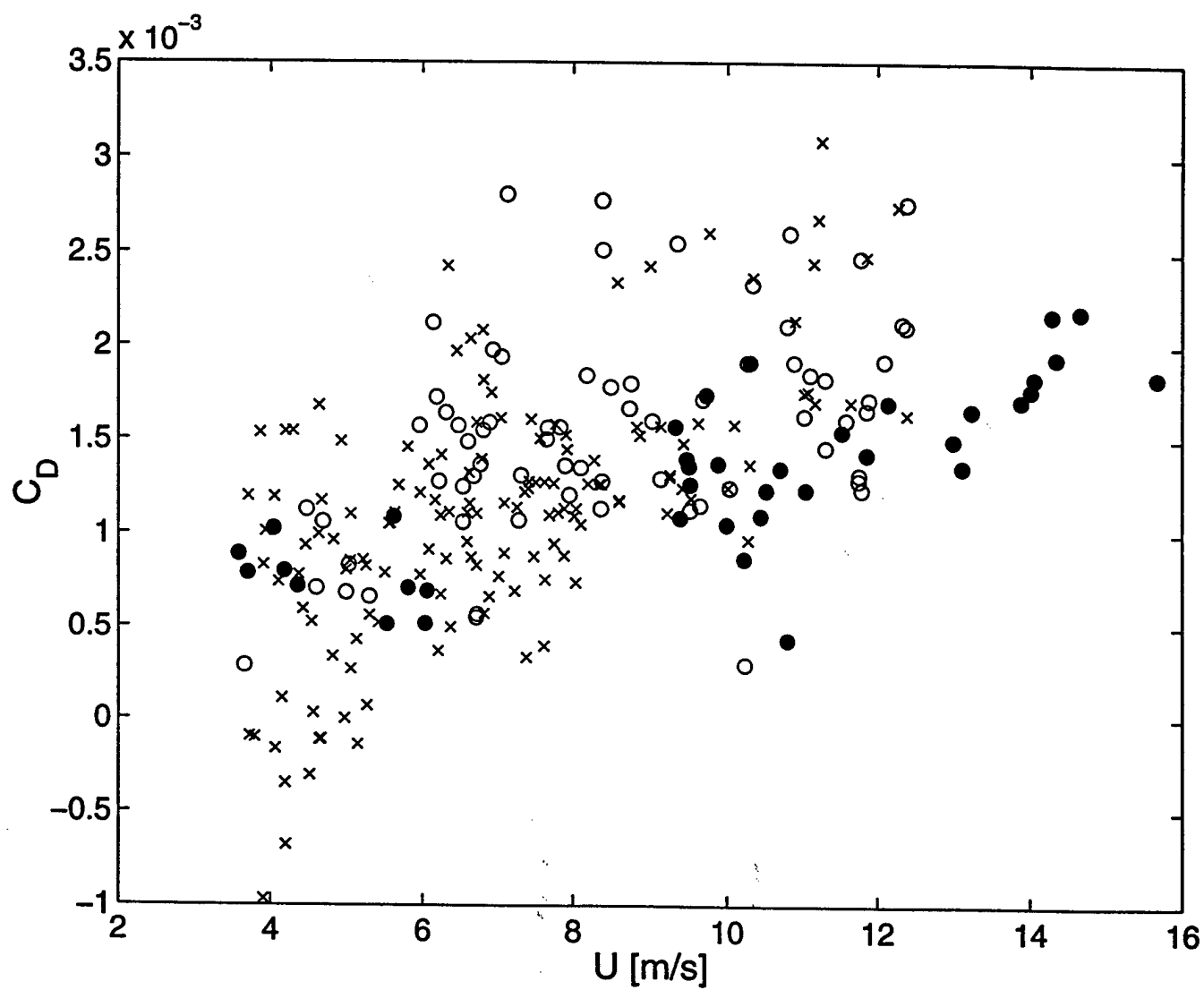
FIG. 14. Bivariate velocity  $uw$  cospectra from swell runs. The data, described in Table 2b, are from the wind speed range  $U \approx 4 - 5\text{ms}^{-1}$ . For the  $\diamond$  data,  $U/c_p = 0.61$ ; for the other data,  $U/c_p < 0.5$ . The solid line is the pure wind sea universal curve, rendered dimensional using the data of pure wind sea run 87176.

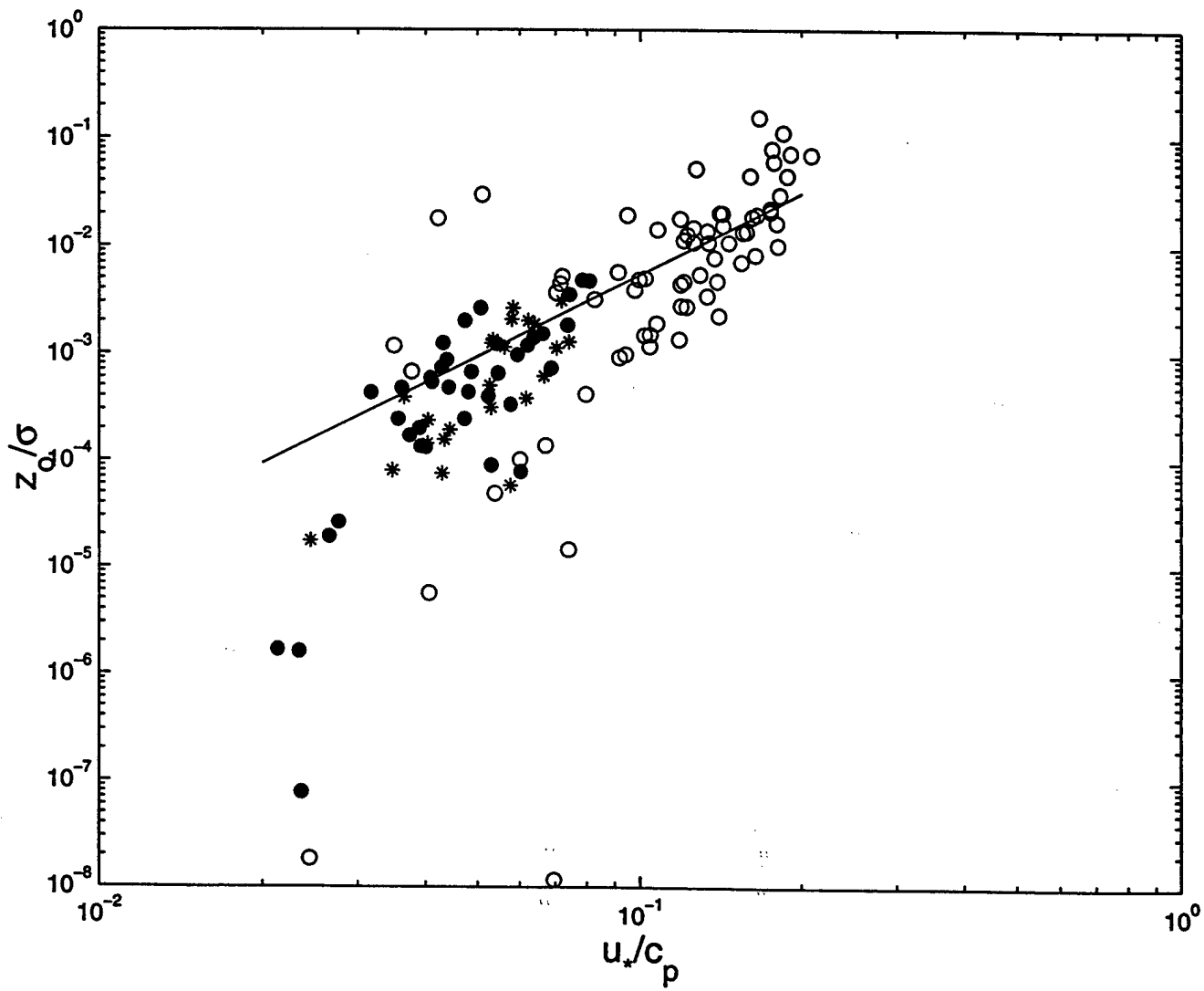
FIG. 15. Bivariate velocity spectra (vertical (a) and horizontal inline (b)) and cospectra (c) from slow swell runs, in the universal scaling of Miyake *et al.* (1970). The data are described in Table 2c. The shaded areas represent  $\pm$  one standard error about the pure wind sea universal curves.

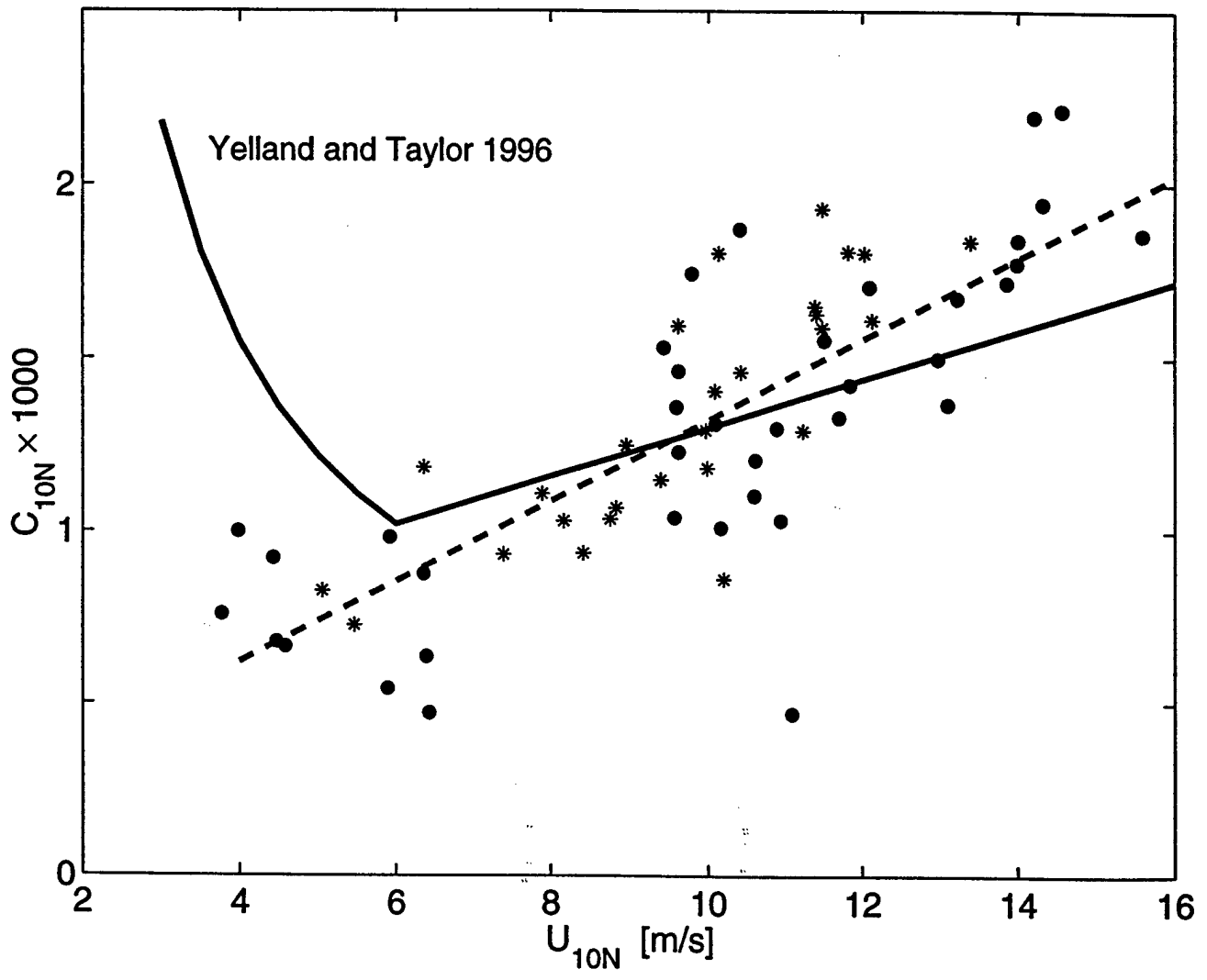


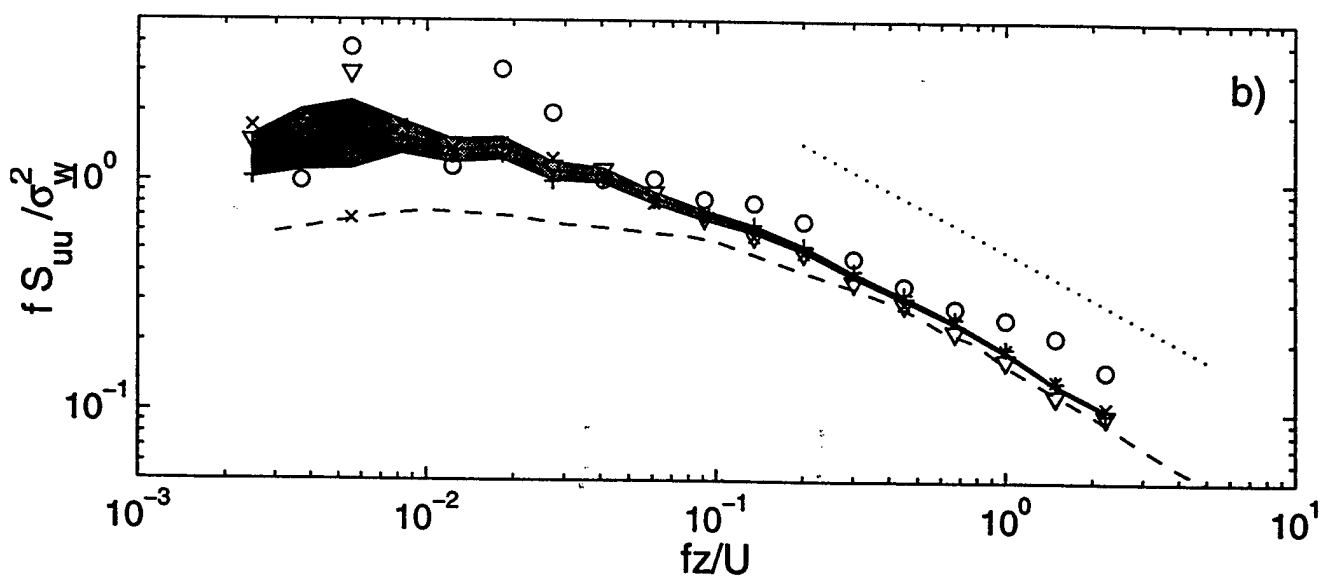
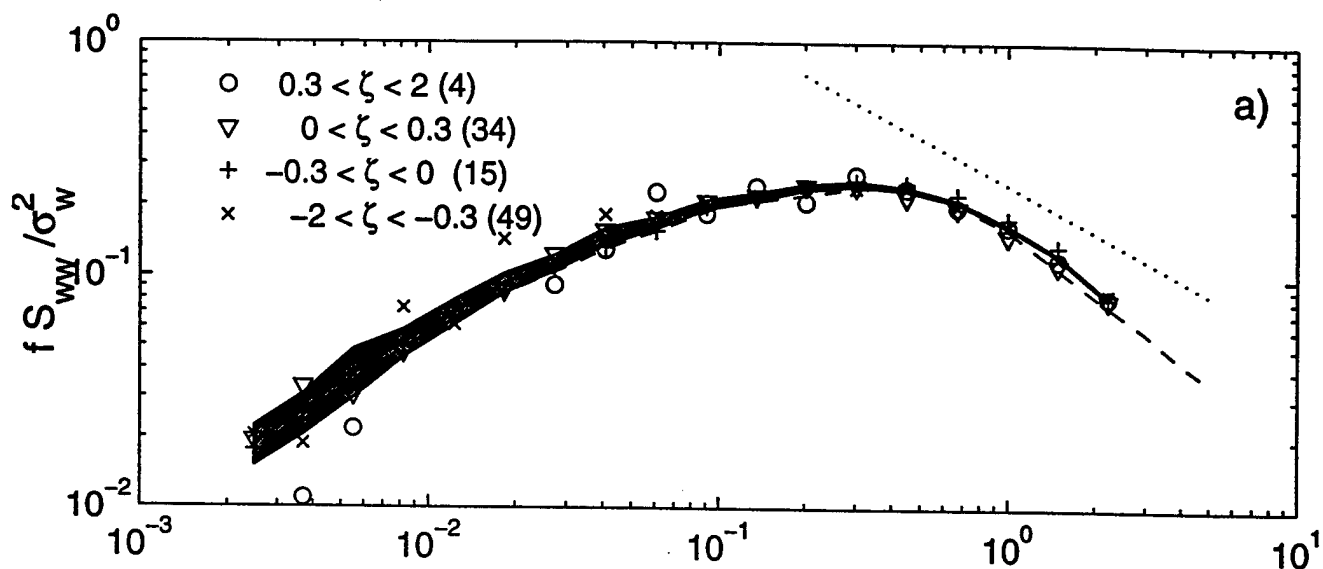












7a,b

